

Odd and even Kondo effects from emergent localization in quantum point contacts

M. J. Iqbal¹, Roi Levy², E. J. Koop¹, J. B. Dekker¹, J. P. de Jong¹, J. H. M. van der Velde¹, D. Reuter³, A. D. Wieck³, Ramón Aguado⁴, Yigal Meir^{2,5} & C. H. van der Wal¹

A quantum point contact (QPC) is a basic nanometre-scale electronic device: a short and narrow transport channel between two electron reservoirs. In clean channels, electron transport is ballistic and the conductance is then quantized as a function of channel width^{1,2} with plateaux at integer multiples of $2e^2/h$ (where e is the electron charge and h is Planck's constant). This can be understood in a picture where the electron states are propagating waves, without the need to account for electron–electron interactions. Quantized conductance could thus be the signature of ultimate control over nanoscale electron transport. However, even studies with the cleanest QPCs generically show significant anomalies in the quantized conductance traces, and there is consensus that these result from electron many-body effects^{3,4}. Despite extensive experimental and theoretical studies^{4–11}, understanding these anomalies is an open problem. Here we report that the many-body effects have their origin in one or more spontaneously localized states that emerge from Friedel oscillations in the electron charge density within the QPC channel. These localized states will have electron spins associated with them, and the Kondo effect—related to electron transport through such localized electron spins—contributes to the formation of the many-body state^{5–7}. We present evidence for such localization, with Kondo effects of odd or even character, directly reflecting the parity of the number of localized states; the evidence is obtained from experiments with length-tunable QPCs that show a periodic modulation of the many-body properties with Kondo signatures that alternate between odd and even Kondo effects. Our results are of importance for assessing the role of QPCs in more complex hybrid devices^{12,13} and for proposals for spintronic and quantum information applications^{14,15}. In addition, our results show that tunable QPCs offer a versatile platform for investigating many-body effects in nanoscale systems, with the ability to probe such physics at the level of a single site.

There are two signatures of many-body physics that are generically observed for a wide variety of QPCs, including systems in GaAs (refs 3, 9), Si (ref. 16) and graphene¹⁷, and that are found for transport of both electrons and holes^{9,16}. First, the quantized conductance traces often show the so-called 0.7 anomaly: an additional small plateau at about $0.7(2e^2/h)$. Second, as a function of bias voltage across the channel, conductance G typically shows a peak around zero bias (named the zero-bias anomaly, ZBA), mostly below the first quantized plateau. The experimental observation⁵ that the ZBA and the 0.7 anomaly had similarities with the Kondo effect for quantum dots (transport through a single localized electron state^{18,19}) inspired theoretical work^{6,7} that proposed that electron many-body physics could lead to localized electrons in the centre of the QPC. This is a remarkable phenomenon, because a QPC is a fully open quantum system. To avoid confusion with localization by an atomic impurity or disordered potential, these many-body states are termed self-consistent or emergent localized states (ELSs).

This theoretical work^{6,7} developed the picture that the many-body effects in QPC channels are intimately related to the occurrence of a

Friedel oscillation—an oscillation in the electron charge density that occurs when electron waves get reflected in a partially open QPC channel—which gets enhanced into an ELS with the charge of about one electron owing to Coulomb repulsion and exchange interactions between electrons. This reduces the conductance and can explain the 0.7 anomaly⁶. However, transport through such a state can be enhanced by the Kondo effect at temperatures below a typical Kondo temperature, T_K . This appears as a ZBA and also moves the 0.7 plateau towards unity (in units of $2e^2/h$), consistent with experiments. This theoretical work^{6,7} also predicted that, depending on parameters, a pair of such ELSs may emerge in the channel, resulting in a double-peak ZBA (as observed in double quantum dots²⁰ owing to the two-impurity Kondo effect^{21–26}). So far no such double-peak ZBAs have been reported for QPCs (Supplementary Information section 3).

We report here the observation of such double-peak ZBAs in a large number of conventional QPCs (with two gate fingers as in Fig. 1a, denoted QPC_{2F}). We also introduce a new type of QPC which has a tunable channel length (with six gate fingers as in Fig. 2a, denoted QPC_{6F}). In these devices, the 0.7 anomaly and the ZBA show a periodic modulation as a function of QPC length, which we attribute to an increasing number of ELSs. Thus, as the number of ELSs increases with QPC length, its parity alternates, giving rise to modulation between Kondo effects for an odd or even number of localized states (known as odd- and even-impurity Kondo effects), and, as a result, between single- and double-peak ZBAs. In addition, the 0.7 anomaly shows a periodic modulation because the enhancement of the 0.7 feature towards unit conductance depends on both the parity and the parameters of the Kondo system such as T_K , and these are both modulated as a function of QPC length.

The signatures of a pair of ELSs are more likely to be observed on shorter QPCs⁷. We thus focused on QPC_{2F} of lithographic length $L = 200$ nm (and width $W = 350$ nm), which is shorter than most QPCs reported in the literature. We searched for double-peak ZBAs in a set of 80 QPC_{2F} (realized in two different wafer materials, different fabrication runs, different cool-downs, and with or without gate-biased cool-down; see Methods) and found them in about half the studied devices. The ubiquity of the phenomenon, and the fact that such double-peak ZBAs were persistently observed in the same devices over different cool-downs, implies that it is a generic effect and not due to a fortuitous impurity nearby. Figure 1 presents data from two QPC_{2F} to illustrate that the signatures of many-body physics show qualitatively similar features, though with significant device-to-device variation (whereas there is no strong variation in the manifestation of non-interacting electron physics, such as the quantized conductance^{8,10}). Figure 1b, c presents measurements of the linear conductance (Methods). In addition to the quantized conductance plateaux at integer multiples of $2e^2/h$, the trace in Fig. 1c shows an additional shoulder at $G \approx 0.7(2e^2/h)$ (the 0.7 anomaly, also observed for the device of Fig. 1b at higher temperatures). Results for the nonlinear conductance (Methods) of these same devices are presented in Fig. 1d, e. Most traces between 0 and $1(2e^2/h)$ show a

¹Zernike Institute for Advanced Materials, University of Groningen, NL-9747AG Groningen, The Netherlands. ²Department of Physics, Ben-Gurion University of the Negev, Beer Sheva 84105, Israel.

³Angewandte Festkörperphysik, Ruhr-Universität Bochum, D-44780 Bochum, Germany. ⁴Instituto de Ciencia de Materiales de Madrid (ICMM), Consejo Superior de Investigaciones Científicas (CSIC), Sor Juana Ines de la Cruz 3, 28049 Madrid, Spain. ⁵Ilse Katz Institute for Nanoscale Science and Technology, Ben-Gurion University of the Negev, Beer Sheva 84105, Israel.

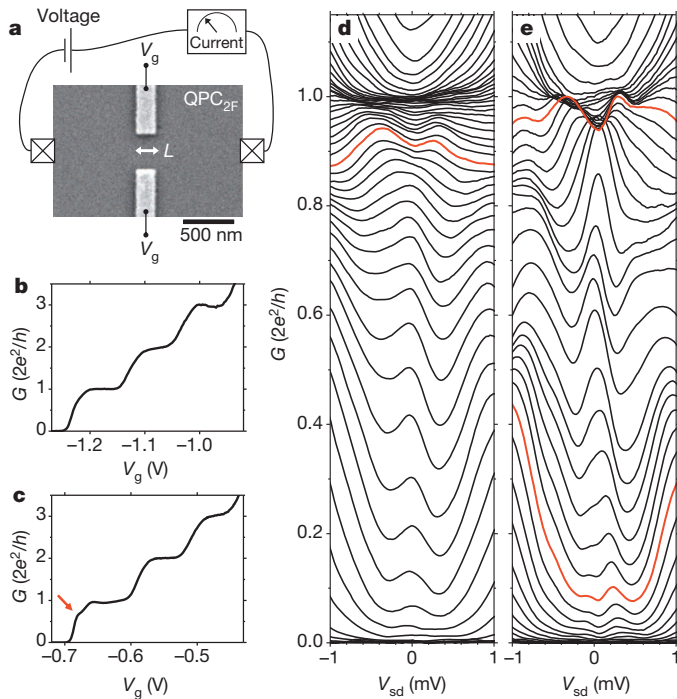


Figure 1 | Conductance of quantum point contacts. **a**, Electron microscope image of a conventional quantum point contact (QPC) with two gate fingers (QPC_{2F}). These gates are on the surface of a wafer with a 2DEG at 110 nm or 114 nm depth. Applying voltages V_g to these gates induces a narrow transport channel between source and drain regions of the 2DEG. The conductance of the QPCs is studied by applying and measuring voltage and current signals on contacts to the 2DEG. For QPC_{2F} the length of the transport channel is fixed by the lithographic length L . **b**, **c**, Linear conductance G measured on two different QPC_{2F} with $L = 200$ nm. The traces show clear quantized conductance plateaux at integer multiples of $2e^2/h$ (the shift in dependence on V_g for **c** as compared to **b** is due to a different cool-down procedure; see Methods). The plateaux and transitions between plateaux show small deviations from clean quantized conductance behaviour, such as an additional shoulder at $G \approx 0.7(2e^2/h)$ in **c** (red arrow). **d**, Nonlinear conductance G as a function of source–drain voltage V_{sd} at various V_g settings, for the device of **b**. The zero-bias anomaly (ZBA, enhanced conductance around $V_{sd} = 0$) has mostly single-peak character, but has double-peak character for $G \approx 0.9(2e^2/h)$ (for example the red trace). **e**, Similar results as **d** for the device of **c**. In this device, ZBAs with double-peak character appear at $G \approx 0.1(2e^2/h)$ and $G \approx 0.95(2e^2/h)$.

single-peak ZBA (the enhancement of conductance within ± 0.5 mV around $V_{sd} = 0$ mV, where V_{sd} is the bias voltage across the channel). However, the red traces mark examples where the ZBA appears with double-peak character (the asymmetric character of these nonlinear conductance traces will be discussed below). For double-peak ZBAs just below $1(2e^2/h)$, we typically observe a peak splitting that increases with conductance.

Theoretical work⁷ predicted that the Friedel oscillation resulting from the screening of the QPC potential would create two electron ‘puddles’, one on each side of the QPC. For most QPC geometries, it showed that lowering the potential by means of the gate voltage would give a single ELS in the centre of the QPC because the Friedel oscillations from both sides connect. However, for short QPCs (for L similar to the Fermi wavelength) the two ELSs remain intact as the potential is lowered. This gives the physics of a two-impurity Kondo system, and as the coupling between them gets stronger with increasing conductance, the ZBA splits^{22–26}. At lower conductance values, the ZBA may appear as a single or a double peak, depending on the ratio between the Kondo temperature of the two ELSs and the strength of interaction between them. Although this is fully consistent with our observations (Fig. 1d, e), the coupling between these ELSs and the resulting splitting of the ZBA depend very sensitively on the device dimensions and the always-present

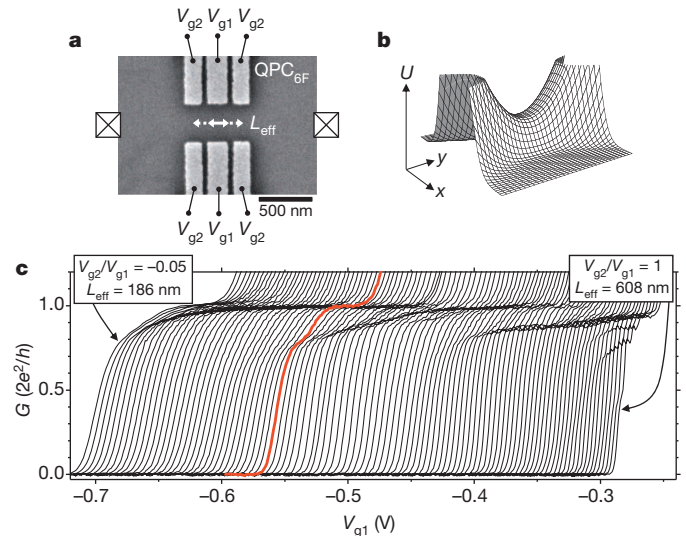


Figure 2 | Length-tunable QPCs. **a**, Electron microscope image of a QPC with six gate fingers (QPC_{6F}). It has a tunable effective length L_{eff} that is set by operating at a fixed ratio V_{g2}/V_{g1} . **b**, Saddle-point potential that illustrates the electron potential energy U (without many-body interactions) in the 2DEG plane in a QPC region. **c**, Linear conductance G as a function of V_{g1} (while co-sweeping V_{g2} at fixed V_{g2}/V_{g1}) measured on a QPC_{6F} for L_{eff} tuned from 186 nm to 608 nm (traces are not offset). In addition to the quantized conductance plateau at $1(2e^2/h)$, most traces show a smaller plateau in the range $0.7(2e^2/h)$ to $0.9(2e^2/h)$ due to many-body effects. For this signature of many-body effects, three periods of modulation can be observed in its dependence on V_{g2}/V_{g1} (that is, L_{eff}).

remote imperfections (Supplementary Information section 4), and this leads to significant variability among devices. Thus, a more stringent test of this picture is possible with QPCs whose parameters can be modified continuously.

We addressed this by investigating a set of eight QPC_{6F} devices, for which we could gradually change the effective channel length L_{eff} of the saddle-point potential. These devices showed qualitatively identical behaviour, with an oscillatory signature of the 0.7 anomaly and regular modulation between single- and double-peak ZBAs with increasing L_{eff} (Fig. 3b, c). These reproducible observations on eight QPC_{6F} (and for different cool-downs of one QPC_{6F}; Supplementary Information section 10) are consistent with the emergence of an increasing number of ELSs due to many-body physics that generically occurs, even in ultra-clean QPC channels.

Figure 2a depicts the QPC_{6F} devices, for which the effective channel length L_{eff} could be tuned continuously. These were operated with the central gate voltage V_{g1} more negative than the side gate voltage V_{g2} , to avoid quantum dot formation. Our analysis shows that in this regime the gates induce a smooth saddle-point potential, despite the narrow gaps between the gate fingers. The effective channel length L_{eff} is set by V_{g2}/V_{g1} (short for V_{g2}/V_{g1} near 0, long for V_{g2}/V_{g1} near 1; see Supplementary Information section 5 for details). Our devices could thus be controlled to have L_{eff} in a range from about 186 nm to 608 nm. Making V_{g1} less negative, at a fixed ratio V_{g2}/V_{g1} , opens the QPC while keeping the length unchanged.

All QPC_{6F} showed clear quantized conductance plateaux. Figure 2c shows for one device how the 0.7 anomaly appears as an additional plateau (smaller than the quantized conductance plateaux) in the range $0.7(2e^2/h)$ to $0.9(2e^2/h)$, and that this plateau shows a dependence on L_{eff} , with three periods of modulation for the range $L_{\text{eff}} = 186$ nm to 608 nm. The nonlinear conductance measurements from this device (Fig. 3a) show how the ZBAs appear for $L_{\text{eff}} = 286$ nm. At a fixed length, the ZBAs alternate between single-peak and double-peak character when opening the QPC, again with increased splitting for the double-peak ZBA as the conductance approaches $1(2e^2/h)$. The overall

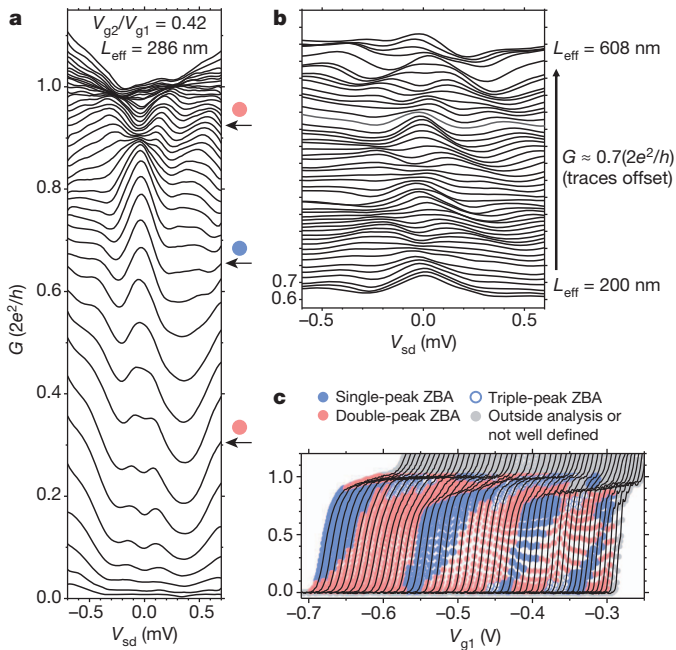


Figure 3 | ZBAs in the nonlinear conductance of a QPC_{6F}. **a**, Nonlinear conductance G as a function of source–drain voltage V_{sd} at various V_{g1} settings, for operation at $L_{eff} = 286$ nm. The ZBA appears alternately with single- or double-peak character. **b**, Evolution of the ZBA in the nonlinear conductance at fixed conductance level of $\sim 0.7(2e^2/h)$ as a function of L_{eff} (traces offset). The ZBA has alternately single- or double-peak character. **c**, The character of the ZBA (single-, double- or triple-peak, as labelled) mapped out on the linear conductance data of Fig. 2c.

appearance of the ZBAs is very similar to that of fixed-length QPC_{2F} (Fig. 1d, e). Figure 3b shows that there is also a modulation between single- and double-peak character when increasing L_{eff} at a fixed conductance level (as evaluated immediately next to the ZBA). Figure 3c plots the data of Fig. 2c again, with coloured data symbols on the traces that mark whether the ZBA at that point has single- or double-peak character (in some cases, we find ZBAs that are best described as triple-peak). The modulation between single-peak and double-peak ZBA as a function of L_{eff} also shows about three periods, and is clearly correlated with the modulation of the 0.7 anomaly.

To critically check the relevance of two-impurity Kondo physics to our observations, we measured the temperature and magnetic field dependence of double-peak ZBAs and compared these with theory for this system. We obtained the theoretical results by calculating the current through a two-impurity Anderson model. For this model, one expects^{22–26} a current that gets enhanced by the Kondo effect when the temperature is lowered from above the Kondo temperature to below it. Depending on the strength of the effective coupling between the impurities relative to the Kondo temperature, the associated ZBA has either single- or double-peak character.

Figure 4a depicts how the nonlinear conductance develops from a background conductance of $0.75(2e^2/h)$ at 3,000 mK into a double-peak ZBA with peak values up to about $0.90(2e^2/h)$ as the temperature is decreased (we used the device of Fig. 3; Supplementary Fig. 9 shows the temperature dependence of the linear conductance). The conductance between the peaks (the linear conductance) has a non-monotonic temperature dependence (Fig. 4b) that is characteristic of two-impurity Anderson physics²⁷. For comparison, insets in Fig. 4a and b depict the results of the theoretical calculations, and show good qualitative agreement. (We note that this description calculates only the Kondo contribution to the current, which yields zero current at high temperatures owing to Coulomb blockade; in contrast, the ELSs in QPCs are not expected to show strong Coulomb blockade at high temperatures but rather a finite background conductance, as observed.) The theoretical

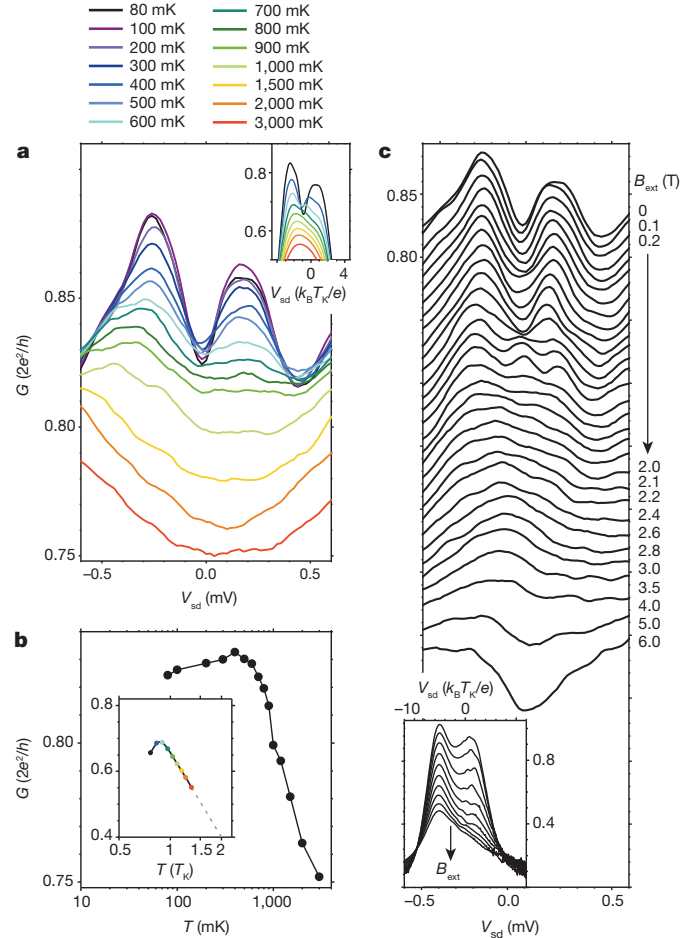


Figure 4 | Comparison between experiments and theory of the Anderson model for a two-impurity Kondo system. **a**, Evolution of the nonlinear conductance (with double-peak ZBA) as a function of temperature for a QPC_{6F} operated with fixed $V_{g1} = -0.528$ V and fixed $V_{g2}/V_{g1} = 0.3$ (traces not offset). Inset, calculated nonlinear-conductance traces from a two-impurity Kondo model (see main text). **b**, The conductance level of the traces in panel **a** near zero bias (between the two ZBA peaks, evaluated at $V_{sd} = -0.02$ mV) as a function of temperature (logarithmic axis). Inset, the same analysis applied to the theoretical results in the inset of **a**. **c**, Evolution of the nonlinear conductance (same device and operation point as **a**) as a function of applied in-plane magnetic field B_{ext} (traces offset by $-0.01(2e^2/h)$). Inset, calculated nonlinear-conductance traces from a two-impurity Kondo model.

traces are calculated for two impurity sites with unequal coupling strength Γ to a neighbouring electron reservoir, and accordingly an unequal Kondo temperature T_K (the plots are presented on an energy scale given by the highest Kondo temperature of the two sites). The asymmetry between the two Γ parameters gives asymmetric double-peak ZBAs, with the minimum conductance between the peaks not exactly at $V_{sd} = 0$, very similar to the experimentally observed double-peak ZBAs. We should expect such asymmetries between the two Γ parameters, because the Γ values depend exponentially on the coupling between the ELSs and the electron reservoirs (Supplementary Information section 4).

Figure 4c presents the measured magnetic field dependence of this double-peak ZBA. Theoretically, one expects different evolutions with magnetic field depending on the relative magnitude of parameters—such as the Kondo temperature of each impurity, the coupling between the impurities, the asymmetry between the impurities and the temperature. The possibilities include each peak splitting into two sub-peaks, the peaks getting closer and merging, and the peaks moving closer and crossing each other. We see such diverse dependence on magnetic field for the different operation points of a given device, and for different

devices. Figure 4c shows one example, with a comparison to the theoretical expectations (other examples are given in Supplementary Information section 8). We see again good qualitative agreement between the theory of the two-impurity model and the experimental observations.

From the width of the peaks in Fig. 4a we can estimate the Kondo temperature T_K , and the splitting between the peaks is equal to twice the effective coupling between the two ELSs. This coupling is here ~ 0.2 meV (a typical value for the larger data set plotted in Fig. 3c). This should be consistent with the temperature at which the double-peak character of the ZBA is no longer resolved (and the temperature where the non-monotonic temperature dependence of conductance has a maximum²⁷). In Fig. 4a, this occurs for ~ 800 mK (that is, ~ 0.1 meV). This is in reasonable agreement with the distance between the peaks. The fact that it is on the low side is probably because T_K is here at the same energy scale as the splitting (~ 0.15 meV when estimated as half the peak widths in Fig. 4a). We also analysed ZBAs with pronounced single-peak character in the same manner as in ref. 5, and found agreement with the single-impurity Kondo model to the same extent.

The increase of L_{eff} that induces one period of modulation for the 0.7 anomaly and the split-peak character of the ZBA in Fig. 3 (~ 100 nm to ~ 150 nm) matches the Fermi wavelength in the QPC channel (Supplementary Information section 6). This supports the hypothesis that the periodicity is linked to Friedel oscillations in the channel which gradually develop additional periods as it gets longer. (That such Friedel oscillations occur on scattering in a two-dimensional electron gas, 2DEG, has been observed directly in a different setting²⁸.) The increasing number of ELSs with channel length leads to alternation between odd- and even-impurity Kondo effects, and to modulation between single-peak and double-peak ZBAs, respectively (the three-impurity case was studied in ref. 29 and can show ZBAs with triple- or predominantly single-peak character).

To support this picture, we carried out numerical spin density functional theory (SDFT) calculations, generalizing earlier work⁷ (Supplementary Information section 2). The length of the channel was determined by a gate of variable length. We studied whether SDFT yields localized states with the charge of about one electron as the state with lowest energy. The results (an example is in Supplementary Fig. 1) show an increasing number of ELSs as the channel gets longer, and also as the QPC is opened by lowering the QPC saddle-point potential at fixed length. These calculations support the picture we have presented here: the number of ELSs increases by one each time the QPC length increases over a range that allows for one additional period of the Friedel oscillation in the QPC channel. The SDFT results suggest that, depending on the overlap of the ELSs, higher spin states ($S = 1$ or $S = 3/2$) may develop in the QPC, making it possible to study Kondo effects for higher spin, and enabling investigation of transport through such exotic states.

The emergence of a ZBA for a hybrid device with a semiconductor channel was recently reported as a signature of Majorana fermions¹². The fact that similar ZBAs occur with rich behaviour in plain semiconductor QPCs suggests that one should be cautious when ruling out alternative explanations for these Majorana signatures¹³. Evidently, basic understanding of the physics in QPCs is a crucial step in understanding more complex hybrid structures. Tunable QPCs offer an excellent new test ground for such studies, and they are also suited for detailed studies of Friedel oscillations³⁰ and strongly correlated electrons in low dimensions, at the level of a single site.

METHODS SUMMARY

Experimental methods. QPCs were realized by locally depleting the 2DEG below the surface of a GaAs/AlGaAs heterostructure (for details, see Methods). In the standard approach, applying negative voltage to two metallic gate fingers on the surface of such material (Fig. 1a) induces an electrostatic potential barrier between a source and drain reservoirs in the 2DEG, with a small tunable opening in the form of a saddle-point potential (Fig. 2b). Such devices with two gate fingers are denoted QPC_{2F} and these have a fixed channel length L . We also studied novel devices with six gate fingers (Fig. 2a), denoted QPC_{6F}, which have a channel with tunable length L_{eff} . We focus on the differential conductance G , which is obtained

by applying and measuring voltage and current signals as in the simplified scheme in Fig. 1a (for details, see Methods). Results for G at zero bias voltage V_{sd} are called here linear conductance, whereas results for G as a function of V_{sd} (bias spectroscopy) are called here nonlinear conductance. Unless stated otherwise, we present data taken at a temperature T of 80 mK and zero magnetic field.

Kondo transport calculations. We obtained the theoretical results by calculating the current through a two-impurity Anderson model within the slave-boson non-crossing approximation²⁷ (detailed in Supplementary Information section 1).

SDFT calculations. We obtained the SDFT results by extending the work of ref. 7 (detailed in Supplementary Information section 2).

Full Methods and any associated references are available in the online version of the paper.

Received 25 May; accepted 19 July 2013.

Published online 28 August 2013.

- van Wees, B. J. *et al.* Quantized conductance of point contacts in a two-dimensional electron gas. *Phys. Rev. Lett.* **60**, 848–850 (1988).
- Wharam, D. A. *et al.* One-dimensional transport and the quantisation of the ballistic resistance. *J. Phys. Chem.* **21**, L209–L214 (1988).
- Thomas, K. J. *et al.* Possible spin polarization in a one-dimensional electron gas. *Phys. Rev. Lett.* **77**, 135–138 (1996).
- Micolich, A. P. What lurks below the last plateau: experimental studies of the $0.7 \times 2e^2/h$ conductance anomaly in one-dimensional systems. *J. Phys. Condens. Matter* **23**, 443201 (2011).
- Cronenwett, S. M. *et al.* Low-temperature fate of the 0.7 structure in a point contact: a Kondo-like correlated state in an open system. *Phys. Rev. Lett.* **88**, 226805 (2002).
- Meir, Y., Hirose, K. & Wingreen, N. S. Kondo model for the “0.7 anomaly” in transport through a quantum point contact. *Phys. Rev. Lett.* **89**, 196802 (2002).
- Rejec, T. & Meir, Y. Magnetic impurity formation in quantum point contacts. *Nature* **442**, 900–903 (2006).
- Koop, E. J. *et al.* The influence of device geometry on many-body effects in quantum point contacts: signatures of the 0.7 anomaly, exchange and Kondo. *J. Supercond. Nov. Magn.* **20**, 433–441 (2007).
- Komijani, Y. *et al.* Evidence for localization and 0.7 anomaly in hole quantum point contacts. *Europhys. Lett.* **91**, 67010 (2010).
- Burke, A. M. *et al.* Extreme sensitivity of the spin-splitting and 0.7 anomaly to confining potential in one-dimensional nanoelectronic devices. *Nano Lett.* **12**, 4495–4502 (2012).
- Wu, P. M., Li, P., Zhang, H. & Chang, A. M. Evidence for the formation of quasibound states in an asymmetrical quantum point contact. *Phys. Rev. B* **85**, 085305 (2012).
- Mourik, V. *et al.* Signatures of Majorana fermions in hybrid superconductor-semiconductor nanowire devices. *Science* **336**, 1003–1007 (2012).
- Churchill, H. O. H. *et al.* Superconductor-nanowire devices from tunneling to the multichannel regime: zero-bias oscillations and magnetoconductance crossover. *Phys. Rev. B* **87**, 241401(R) (2013).
- Bertoni, A., Bordone, P., Brunetti, R., Jacoboni, C. & Reggiani, S. Quantum logic gates based on coherent electron transport in quantum wires. *Phys. Rev. Lett.* **84**, 5912–5915 (2000).
- Blaauboer, M. & DiVincenzo, D. P. Detecting entanglement using a double-quantum-dot turnstile. *Phys. Rev. Lett.* **95**, 160402 (2005).
- Bagraev, N. T., Shelykh, I. A., Ivanov, V. K. & Klyachkin, L. E. Spin depolarization in quantum wires polarized spontaneously in zero magnetic field. *Phys. Rev. B* **70**, 155315 (2004).
- Tombros, N. *et al.* Quantized conductance of a suspended graphene nanoconstriction. *Nature Phys.* **7**, 697–700 (2011).
- Goldhaber-Gordon, D. *et al.* Kondo effect in a single-electron transistor. *Nature* **391**, 156–159 (1998).
- Cronenwett, S. M., Oosterkamp, T. H. & Kouwenhoven, L. P. A tunable Kondo effect in quantum dots. *Science* **281**, 540–544 (1998).
- Jeong, H., Chang, A. M. & Melloch, M. R. The Kondo effect in an artificial quantum dot molecule. *Science* **293**, 2221–2223 (2001).
- Jones, B. A., Kotliar, B. G. & Millis, A. J. Mean-field analysis of 2 antiferromagnetically coupled Anderson impurities. *Phys. Rev. B* **39**, 3415–3418 (1989).
- Ivanov, T. The nonlinear conductance of a double quantum dot in the Kondo regime. *Europhys. Lett.* **40**, 183–188 (1997).
- Pohjola, T. *et al.* Resonant tunneling through a two-level dot and double quantum dots. *Europhys. Lett.* **40**, 189–194 (1997).
- Aono, T., Eto, M. & Kawamura, K. Conductance through quantum dot dimer below the Kondo temperature. *J. Phys. Soc. Jpn* **67**, 1860–1863 (1998).
- Georges, A. & Meir, Y. Electronic correlations in transport through coupled quantum dots. *Phys. Rev. Lett.* **82**, 3508–3511 (1999).
- Aguado, R. & Langreth, D. C. Out-of-equilibrium Kondo effect in double quantum dots. *Phys. Rev. Lett.* **85**, 1946–1949 (2000).
- Aguado, R. & Langreth, D. C. Kondo effect in coupled quantum dots: a noncrossing approximation study. *Phys. Rev. B* **67**, 245307 (2003).
- Kanisawa, K., Butcher, M. J., Yamaguchi, H. & Hirayama, Y. Imaging of Friedel oscillation patterns of two-dimensionally accumulated electrons at epitaxially grown InAs(111)A surfaces. *Phys. Rev. Lett.* **86**, 3384–3387 (2001).
- Vernek, E. *et al.* Kondo regime in triangular arrangements of quantum dots: molecular orbitals, interference, and contact effects. *Phys. Rev. B* **80**, 035119 (2009).

30. Simion, G. E. & Giuliani, G. F. Friedel oscillations in a Fermi liquid. *Phys. Rev. B* **72**, 045127 (2005).

Supplementary Information is available in the online version of the paper.

Acknowledgements We thank B. J. van Wees, A. Aqeel, S. Ludwig, J. von Delft and Y. Komijani for discussions and B. Wolfs, J. Holstein and M. de Roosz for technical assistance. We acknowledge financial support from the German programmes DFG-SPP 1285, Research School Ruhr-Universität Bochum and BMBF QuaHL-Rep 16BQ1035, and grants FIS2009-08744 and FIS2012-33521 from the Spanish Ministry of Economy and Innovation. M.J.I. acknowledges a scholarship from the Higher Education Commission of Pakistan. Y.M. and R.L. acknowledge support from the ISF.

Author Contributions M.J.I. was the lead researcher for experiments, with C.H.v.d.W. as supervisor, experimental contributions from E.J.K., J.B.D., J.P.d.J. and J.H.M.v.d.V., and design contributions from Y.M. The devices were fabricated from wafer material that was grown by D.R. and A.D.W. The calculations of electron transport in Kondo systems were carried out by R.A. The SDFT contribution was worked out by R.L. with Y.M. as supervisor. M.J.I., C.H.v.d.W. and Y.M. wrote the paper.

Author Information Reprints and permissions information is available at www.nature.com/reprints. The authors declare no competing financial interests. Readers are welcome to comment on the online version of the paper. Correspondence and requests for materials should be addressed to M.J.I. (m.j.iqbal@rug.nl) or C.H.v.d.W. (c.h.van.der.wal@rug.nl).

METHODS

Materials and device fabrication. QPC devices were fabricated with two different GaAs/AlGaAs heterostructures containing a 2DEG in a heterojunction quantum well. They were grown by molecular-beam epitaxy under similar conditions, and the properties of the 2DEGs were similar. We obtained very similar results with both materials. Most of the results presented in this Letter come from material 2, only the data in Fig. 1b, d comes from material 1.

Material 1 was a GaAs/Al_{0.32}Ga_{0.68}As heterostructure with a 2DEG 114 nm below the surface. The electrons of the 2DEG were supplied by modulation doping with Si at about $1 \times 10^{24} \text{ m}^{-3}$. At 4.2 K, the mobility of the 2DEG was $\mu = 159 \text{ m}^2 \text{ V}^{-1} \text{ s}^{-1}$, and the electron density $n_s = 1.5 \times 10^{15} \text{ m}^{-2}$ after cooling down in the dark. The layer with modulation doping started at 37 nm distance from the 2DEG position towards the wafer surface (this material was uniquely used in the related results presented in ref. 8).

Material 2 was a GaAs/Al_{0.35}Ga_{0.65}As heterostructure with a 2DEG 110 nm below the surface. This material also had modulation doping with Si at about $1 \times 10^{24} \text{ m}^{-3}$. At 4.2 K, the mobility of the 2DEG was $\mu = 118 \text{ m}^2 \text{ V}^{-1} \text{ s}^{-1}$, and the electron density $n_s = 1.60 \times 10^{15} \text{ m}^{-2}$. Here the layer with modulation doping started at 45 nm distance from the 2DEG position.

QPCs were realized by locally depleting the 2DEG below the surface of the GaAs/AlGaAs heterostructures. In the standard approach, applying negative voltage V_g to two metallic gate fingers on the surface of such material (Fig. 1a) induces an electrostatic potential barrier between source and drain reservoirs in the 2DEG, with a small tunable opening in the form of a saddle-point potential (Fig. 2b). Such devices with two gate fingers are denoted QPC_{2F} and these have a fixed channel length L . We also studied novel devices with six gate fingers (Fig. 2a), denoted QPC_{6F}, which have a channel with tunable length L_{eff} . Tuning of V_g on the gates allows for controlling the effective QPC shape (for details, see Supplementary Information section 5).

The depletion gates were defined with standard electron-beam lithography and lift-off techniques and by depositing 15 nm of Au with a Ti sticking layer. The reservoirs were connected to macroscopic leads via ohmic contacts, which were realized by annealing a thin Au/Ge/Ni layer that was deposited on the surface. Part of our data (including all the results presented in the main text, except for the data in Fig. 1b, d) was obtained after cooling down with about +0.3 V on the gates to suppress $1/f$ and telegraph noise in the conductance signals due to charge instabilities

in the doping layer (Supplementary Information section 4). We obtained (apart from the change in noise properties) similar results for the cases with and without biased cool-down.

Measurement techniques and set-up. The measurements focus on the differential conductance G , which is obtained by applying and measuring voltage and current signals as in the simplified scheme in Fig. 1a. Results for G at zero bias voltage V_{sd} are called linear conductance, while results for G as a function of V_{sd} (bias spectroscopy) are called nonlinear conductance. Unless stated otherwise, the presented data were taken at a temperature T of 80 mK and zero magnetic field.

The presented results of linear and nonlinear conductance measurements all concern the differential conductance $G = dI/dV_{\text{sd}}$ (where I is the measured current). For linear conductance measurements, we used standard lock-in techniques (typically at 387 Hz), with an a.c. voltage bias $V_{\text{sd}} = V_{\text{ac}} = 10 \mu\text{V}$. For the nonlinear conductance measurements, we superimposed an a.c. and a d.c. voltage bias, $V_{\text{sd}} = V_{\text{dc}} + V_{\text{ac}}$. We used an effective four-terminal measurement where we locally measured the source–drain voltage drop V_{sd} across the QPC, such that we can present results without significant contributions from series resistance. Only one of the source–drain contacts was connected to the grounded shielding of our set-up, and all gate voltages were applied with respect to this ground.

Measurements were performed in a dilution refrigerator with the sample at temperatures from ~ 5 mK to 4.2 K. For all our data, the temperature dependence saturated when cooling below ~ 80 mK. This is consistent with independent measurements of the lowest effective electron temperature that could be achieved with this set-up. The electron temperature of 80 mK allows for probing peak structures in nonlinear conductance traces as narrow as $4k_{\text{B}}T/e = 0.03$ mV (k_{B} is Boltzmann's constant).

The in-plane magnetic field was applied both parallel and perpendicular to the current direction and we measured devices with the current along the [110] direction and also along the $[-110]$ direction of the crystal, but the results did not depend significantly on these orientations. Alignment of the sample with the magnetic field was within 1° , as determined from Hall voltage measurements on the 2DEG.

Kondo transport calculations. We obtained the theoretical results by calculating the current through a two-impurity Anderson model within the slave-boson non-crossing approximation²⁷ (detailed in Supplementary Information section 1).

SDFT calculations. We obtained the SDFT results by extending the work of ref. 7 (detailed in Supplementary Information section 2).